PL-TR-94-2267

# DEVELOPMENT OF IMPROVED GEOPHYSICAL IMAGING TECHNIQUES FOR ENVIRONMENTAL SITE CHARACTERIZATION

Robert J. Greaves
Jung Mo Lee
David P. Lesmes
M. Nafi Toksöz

Earth Resources Laboratory
Department of Earth, Atmospheric, and Planetary Sciences
Massachusetts Institute of Technology
Cambridge, MA 02139

DTIC
ELECTE
FEB. 0 9 1995
S   D
B

8 October 1994

19950203 389

Scientific Report No. 1
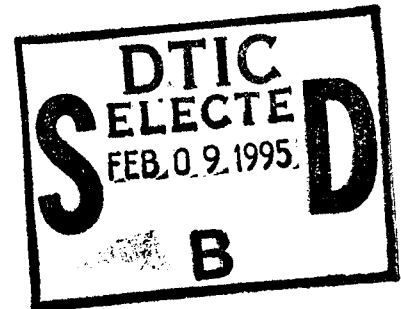
PHILLIPS LABORATORY
Directorate of Geophysics
AIR FORCE MATERIEL COMMAND
HANSCOM AIR FORCE BASE, MA 01731-3010

The views and conclusions contained in this document are those of the authors and should not be interpreted as representing the official policies, either express or implied, of the Air Force or the U.S. Government.

This technical report has been reviewed and is approved for publication.

JAMES F. LEWKOWICZ
Contract Manager
Earth Sciences Division

JAMES F. LEWKOWICZ, Director
Earth Sciences Division

This report has been reviewed by the ESC Public Affairs Office (PA) and is releasable to the National Technical Information Service (NTIS).

Qualified requestors may obtain additional copies from the Defense Technical Information Center. All others should apply to the National Technical Information Service.

If your address has changed, or if you wish to be removed from the mailing list, or if the addressee is no longer employed by your organization, please notify PL/TSI, 29 Randolph Road, Hanscom AFB, MA 01731-3010. This will assist us in maintaining a current mailing list.

Do not return copies of this report unless contractual obligations or notices on a specific document requires that it be returned.

REPORT DOCUMENTATION PAGE

Public reporting burden for this collection of information is estimated to average 1 hour per response, including the time for reviewing instructions, searching existing data sources, gathering and maintaining the data needed, and completing and reviewing the collection of information. Send comments regarding this burden estimate or any other aspect of this collection of information, including suggestions for reducing this burden, to Washington Headquarters Services, Directorate for Information Operations and Reports, 1215 Jefferson Davis Highway, Suite 1204, Arlington, VA 22202-4302, and to the Office of Management and Budget, Paperwork Reduction Project (0704-0188), Washington, DC 20503.

1. AGENCY USE ONLY (Leave blank)	2. REPORT DATE 8 OCT 1994	3. REPORT TYPE AND DATES COVERED Scientific No. 1

4. TITLE AND SUBTITLE
Development of Improved Geophysical Imaging Techniques for Environmental Site Characterization

5. FUNDING NUMBERS
F19628-93-K-0027
PE 62101F
PR 7600
TA GN
WU AD

6. AUTHOR(S)
Robert J. Greaves
Jung Mo Lee
David P. Lesmes   M. Nafi Toksöz

7. PERFORMING ORGANIZATION NAME(S) AND ADDRESS(ES)
Earth Resources Laboratory
Dept. of Earth, Atmospheric, and Planetary Sciences
Massachusetts Institute of Technology
77 Massachusetts Avenue
Cambridge, MA 02139

8. PERFORMING ORGANIZATION REPORT NUMBER
60454

9. SPONSORING/MONITORING AGENCY NAME(S) AND ADDRESS(ES)
Phillips Laboratory
29 Randolph Road
Hanscom AFB, MA 01731-3010

Contract Manager: James F. Lewkowicz/GPEH

10. SPONSORING/MONITORING AGENCY REPORT NUMBER
PL-TR-94-2267

11. SUPPLEMENTARY NOTES

12a. DISTRIBUTION/AVAILABILITY STATEMENT

Approved for Public Release; Distribution Unlimited

12b. DISTRIBUTION CODE

13. ABSTRACT (Maximum 200 words)

The common midpoint (CMP) processing technique has been shown to be effective in improving the results of ground penetrating radar profiling. When radar data are collected with the CMP multi-offset geometry, stacking increases the signal-to-noise ratio of subsurface radar reflections and the effective penetration depth. An important aspect of CMP processing is normal moveout velocity analysis. Most, if not all, GPR surveys, are very limited in spatial extent and the common perception is that within the survey range, radar velocity in the shallow subsurface has very slow or no lateral variation. Therefore, a single velocity function might be considered adequate to describe the subsurface. In this study we show that, in fact, lateral variation in radar velocity can be quite significant and that the stacked profile improves as the number of velocity analysis locations is increased, up to some practical limit.

Interval velocity can be calculated from the normal moveout velocities derived in the CMP velocity analysis. An approximate relationship between interval velocity and water content is derived. By collecting GPR data in the multi-offset CMP geometry, not only is the radar profile improved but it also allows for an interpretation of subsurface variation in water content.

14. SUBJECT TERMS
Ground penetrating radar; velocity analysis; site characterization

15. NUMBER OF PAGES
44

16. PRICE CODE

17. SECURITY CLASSIFICATION OF REPORT	18. SECURITY CLASSIFICATION OF THIS PAGE	19. SECURITY CLASSIFICATION OF ABSTRACT	20. LIMITATION OF ABSTRACT
UNCLASSIFIED	UNCLASSIFIED	UNCLASSIFIED	SAR

NSN 7540-01-280-5500

DTIC QUALITY INSPECTED

Standard Form 298 (Rev. 2-89)
Prescribed by ANSI Std. Z39-18
298-102

TABLE OF CONTENTS

LIST OF ILLUSTRATIONS

Acknowledgments

The authors would like to thank Dr. Peter Annan of Sensors & Software, Inc. for permission to use these data and for several useful discussions about GPR.

List of Contributing Scientists

Robert J. Greaves, Graduate Research Assistant, MIT-Woods Hole Oceanographic Institution Joint Program

Jung Mo Lee, Founding Member Postdoctoral Fellow, Massachusetts Institute of Technology

David P. Lesmes, Postdoctoral Associate, Massachusetts Institute of Technology

M. Nafi Toksöz, Professor of Geophysics, Massachusetts Institute of Technology

List of Current Related Projects

NIEHS Grant NIH-5P42ES0465-08, Geophysical site characterization of the Aberjona Watershed.

EPA Grant CR821516-01-0, Four-dimensional electrical imaging of subsurface contaminants with applications to a controlled spill: a collaborative proposal.

DOE Grant DE-FG02-93ER14322, Electroseismic characterization of lithology and fluid type in the shallow subsurface.

Bibliography of Publications Totally or Partially Sponsored by the Contract

Greaves, R.J., J.M. Lee, D.P. Lesmes, and M.N. Toksöz, Lateral velocity variations and water content estimated from multi-offset ground-penetrating radar, submitted to *Geophysics*, 1994.

Haartsen, M.W. and R.S. Pride, Modeling of coupled electroseismic wave propagation from point sources in layered media, *SEG Expanded Abstracts*, 1994.

Zhao, X., Effects of heterogeneities on fluid flow and borehole permeability, Ph.D. Thesis, Massachusetts Institute of Technology, 1994.

LATERAL VELOCITY VARIATIONS AND WATER CONTENT ESTIMATED FROM MULTI-OFFSET GROUND PENETRATING RADAR

Introduction

Ground penetrating radar (GPR) is the recording of high frequency electromagnetic waves that have reflected from subsurface contrasts in dielectric constant. In low-loss media, ground penetrating radar is capable of producing high resolution images of the shallow subsurface, compared to other surface electric or seismic geophysical techniques. Most commonly, GPR data is collected with a single source-to-receiver offset, usually a minimum offset. In the early development of GPR, multi-offset common midpoint (CMP) sounding was borrowed from reflection seismology as an effective technique for determining glacial ice velocities (Gudmandsen, 1971). As the use of GPR expanded to rock and soil surveys, multi-offset radar sounding has continued to be used primarily for velocity sounding at one or just a few points along a survey line. The advantages of determining velocity with this method are that it requires no prior knowledge of the subsurface, is not intrusive, uses the radar data acquisition system only and can determine the velocity anywhere within the survey. The disadvantage is that acquiring multi-offset data with current GPR systems is slow (compared to zero-offset surveys), or impossible, for systems with fixed source-receiver offset.

Recent case studies have shown that when an entire GPR survey is acquired with the

CMP geometry, multi-trace reflection seismic processing techniques can be used to improve the subsurface radar images (Fisher *et al.,* 1992; Gerlitz *et al.,* 1993). When the data are collected in this configuration, normal moveout velocity analysis is used to derive a continuous 2-D radar stacking velocity field. In general, lateral radar velocity variation has been considered to be small within the spatial range of most surveys. In this study, we show that, in fact, lateral variation in radar velocity can be significant and further, that with increasing lateral velocity description comes improvement in the results of multi-offset radar processing.

In general, ground penetrating radar velocity decreases rapidly with depth (Davis and Annan, 1989). This is primarily a result of increasing water content. Topp *et al.* (1980), derived an empirical relationship between radar propagation velocity and water content. Using this relationship we can estimate water content from the interval velocities calculated from normal moveout velocities. This interpretation increases the potential uses of radar profiling in ground water studies and contaminant spill monitoring. Radar interval velocity can be used to estimate water content when the subsurface is sufficiently resistive to be treated as a low-loss media. This is a reasonable assumption where radar signals penetrate the subsurface to depths of meters or tens of meters. In partially saturated soils, water content may be interpreted as an indicator of saturation. In fully saturated soils, variations in water content can be interpreted as variations in water filled porosity. The improvement to the continuity and depth-of-penetration of the radar image combined with such interpretations of the ve-

locity should encourage the development of GPR systems capable of acquiring multi-offset common midpoint data efficiently for standard surveying.

Multi-offset Data

We obtained a multi-offset GPR survey from Sensors & Software, Inc., that was acquired at the Chalk River research area, operated by Atomic Energy of Canada, Limited. The data were acquired in a cooperation of Sensors & Software Inc., the Atomic Energy of Canada, Ltd. and the UT-Dallas Geophysical Consortium. The data were collected with multiple source antenna to receiver antenna offsets, such that after re-arrangement, 1800 CMP's spaced every 0.25 m were defined. The data were acquired using a pulseEKKO IV digital radar system with 100 MHz antennas. A detailed description of acquisition geometry and data recording parameters can be found in Fisher *et al.* (1992). For these data, each CMP gather has, on average, ten traces with offsets ranging from 0.5 m to 20.0 m. The standard GPR data set would have only a single offset trace at each survey station, usually a minimum offset. In Figure 1, the minimum offset trace profile from the Chalk River data set is displayed. This shows the data as it would be collected in a single offset GPR survey at this site. The subsurface at the site is described as bedrock covered by glacial till and fluvial sand deposits (Davis and Annan, 1989; Fisher *et al.*, 1992). In this profile we see a strong channel shaped reflector that appears to be the depth-of-penetration limit. Also, there is a clear decrease in reflection continuity between about 100–400 nanoseconds from
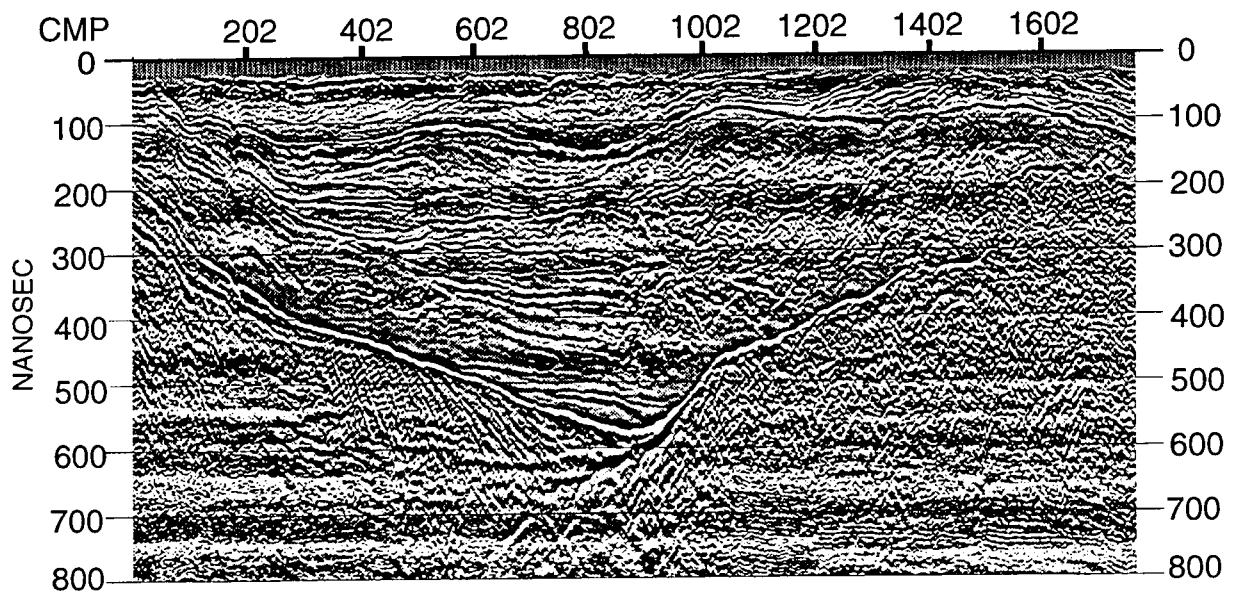
Figure 1: Minimum offset profile extracted from multi-offset GPR data at Chalk River.

CMP 900 to CMP 1800. Improvements to the radar image in these areas, in particular, are observed in the final CMP processed data profiles.

Figure 2a shows a number of CMP gathers with traces arranged in offset order from 0.5 m to 20.0 m within each CMP. Some of the approximately hyperbolic arrivals from reflections are clearly distinguished, but the signal-to-noise is low in this raw data. Pre-processing steps were applied to the data to prepare it for velocity analysis and stacking. The data were bandpass filtered, a top mute (in shot gather mode) was applied to remove the direct arrivals, and time dependent scaling was used to partially correct for geometric spreading loss. A filter in the frequency domain was applied to remove some spatial aliasing effects. AGC (automatic gain control) scaling is used for display. Figure 2b shows the same CMP gathers after these processes have been applied. These filtered data are used in the normal moveout velocity analysis.

Normal Moveout Velocity Estimation

Since the data in this survey were all collected with the CMP geometry, normal moveout (NMO) velocity analysis can be applied at any or all of the CMP's to define the subsurface velocity. How many velocity analyses are required depends on how strongly the radar velocity varies laterally. There is no rule or formula for determining an optimum number of velocity analyses for processing a CMP data set, so this parameter must be established by testing the data itself. In this example, we show how increasing the number of velocity analyses
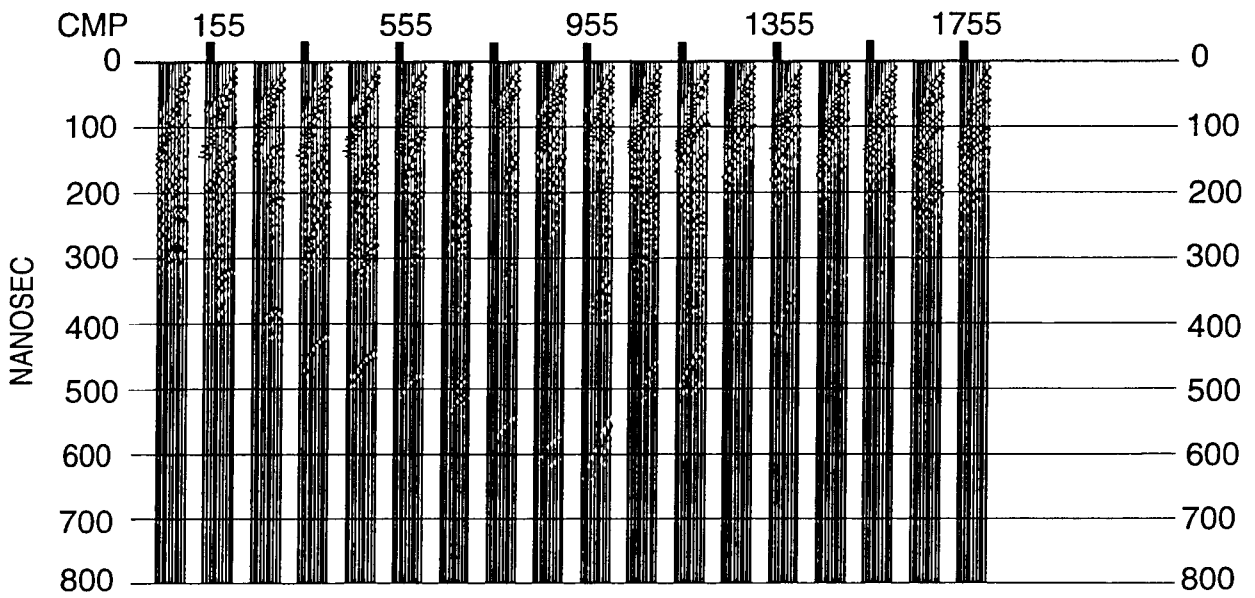
Figure 2a: Radar CMP gathers in offset order before pre-processing. Offsets vary from 0.5 m to 20.0 m within each CMP.
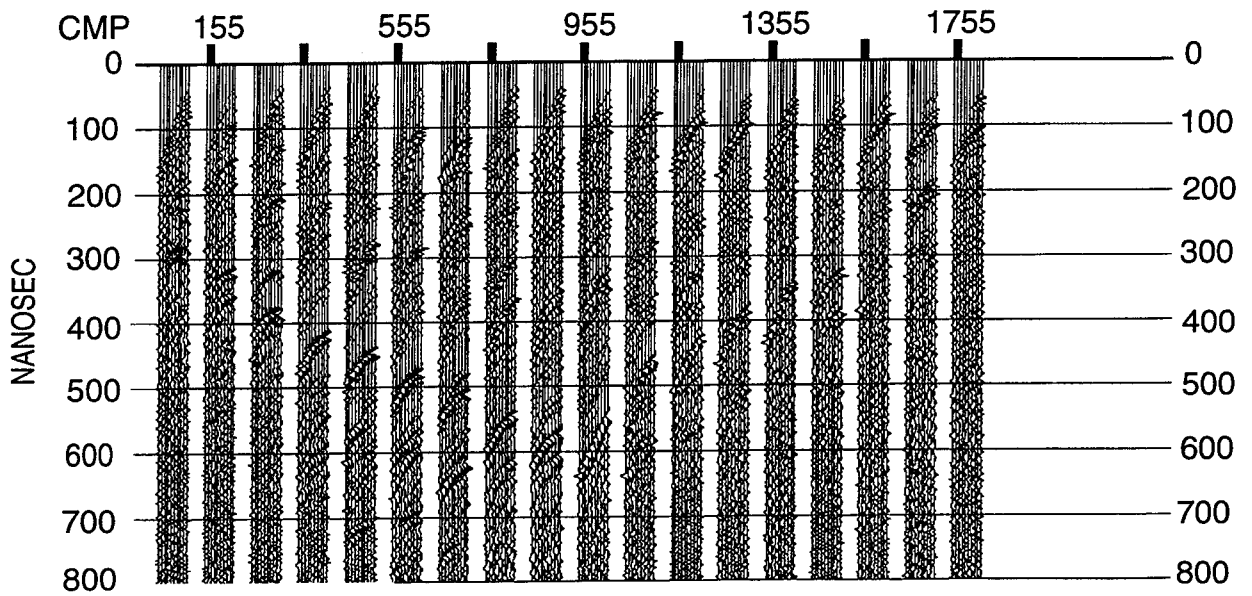
Figure 2b: Radar CMP gathers after pre-processing. Offsets vary from 0.5 m to 20.0 m within each CMP.

affects the final CMP stacked image.

There are a variety of schemes used in NMO velocity analysis (Yilmaz, 1987). We have used a semblance amplitude approach where the data in the CMP's are normal moveout corrected and stacked using a range of trial velocities. The amplitudes versus time over the whole range are then contoured and displayed as a velocity spectrum. The peaks of the amplitude mapping are chosen to define the 1-D velocity function at each CMP being analyzed. After a number of velocity functions have been defined, a 2-D velocity profile is created by interpolation. For a statistical method, like semblance mapping, the more traces there are in any individual CMP, and the larger the offset range (within the small spread approximation), the better the resolution in the velocity spectrum. In practice, the vertical resolution of NMO velocity analysis has limits such that only the highest amplitude velocity spectra peaks are picked for the traveltime versus velocity function. Therefore, the NMO velocity function will usually have less velocity layers defined than there are reflections observed in the data.

When the number of traces per gather is small and somewhat noisy, we expect the velocity spectra to have a relatively poor signal-to-noise ratio. For the Chalk River data we reduce the noise in the velocity spectra by combining, and sorting by offset, the traces from twenty CMP's centered around each CMP chosen for velocity analysis. A typical velocity spectrum, for a single CMP (no combination) is shown in Figure 3a. When the spectrum of the combined 20 CMP's is found, as shown in Figure 3b, the velocity peaks are much better
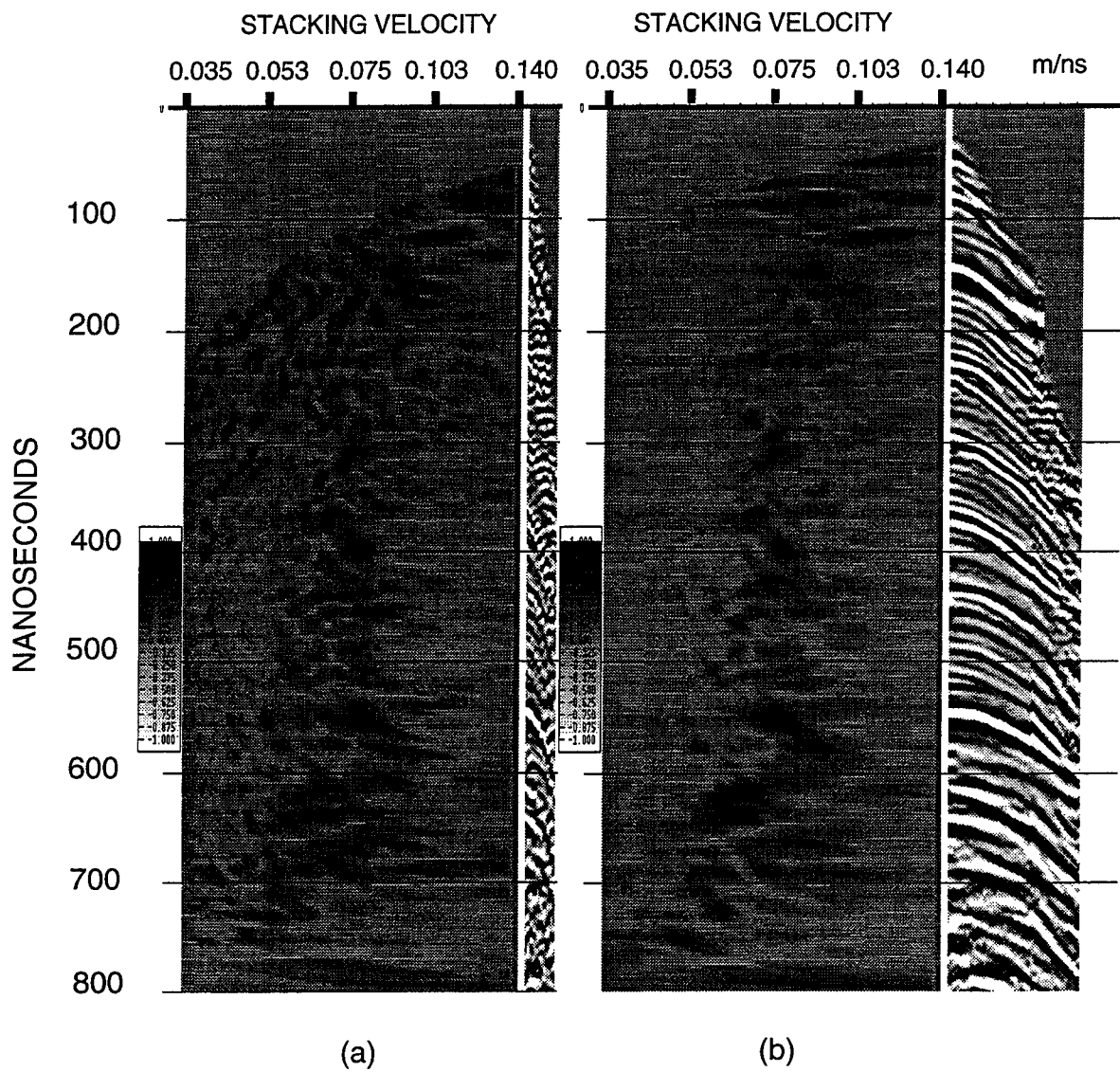
Figure 3: (a) Velocity spectrum of CMP 755. (b) Velocity spectrum of the combination of 20 CMP's centered on CMP 755.

resolved and NMO velocity can be picked with more confidence. To an extent, resolution in the spectra seems to improve with increasing traveltime. This is due in part to the fact that for near surface reflections, the further offset traces are muted and do not contribute to the analysis, so there are less data in the statistical analysis. Secondly, for a constant test velocity interval, changes in stacking occur more slowly as velocity increases, leading, in radar data, to less well resolved peaks in the spectra of near surface reflections. Overall width of the velocity spectra peaks in Figure 3b indicate that resolution of the stacking velocity is on the order of $+/- 0.01 \ m/ns$.

Velocity analyses were performed at regular intervals along the profile. Figure 4 shows the interpolated NMO velocity fields as the number of velocity analyses is increased. Figure 4a is the simple flat layered profile that results when only one CMP is analyzed. Velocity varies from about .125 m/ns near the surface to about .06 m/ns for deep reflectors. The deepest reflectors for which velocity is estimated is at about 750 ns in the central portion of the data. Figure 4b shows the 2-D velocity profile when velocity analyses at four CMP's are included. We see that there is significant lateral variation which approximately mirrors the sediment wedge in the reflection data. Figure 4c includes velocity analyses at nine CMP's, Figure 4d at eighteen CMP's and Figure 4e at 35 CMP's. As the number of velocity analyses increase the velocity field becomes more complicated and suggests that some subsurface properties not directly related to layering are affecting the velocity structure.
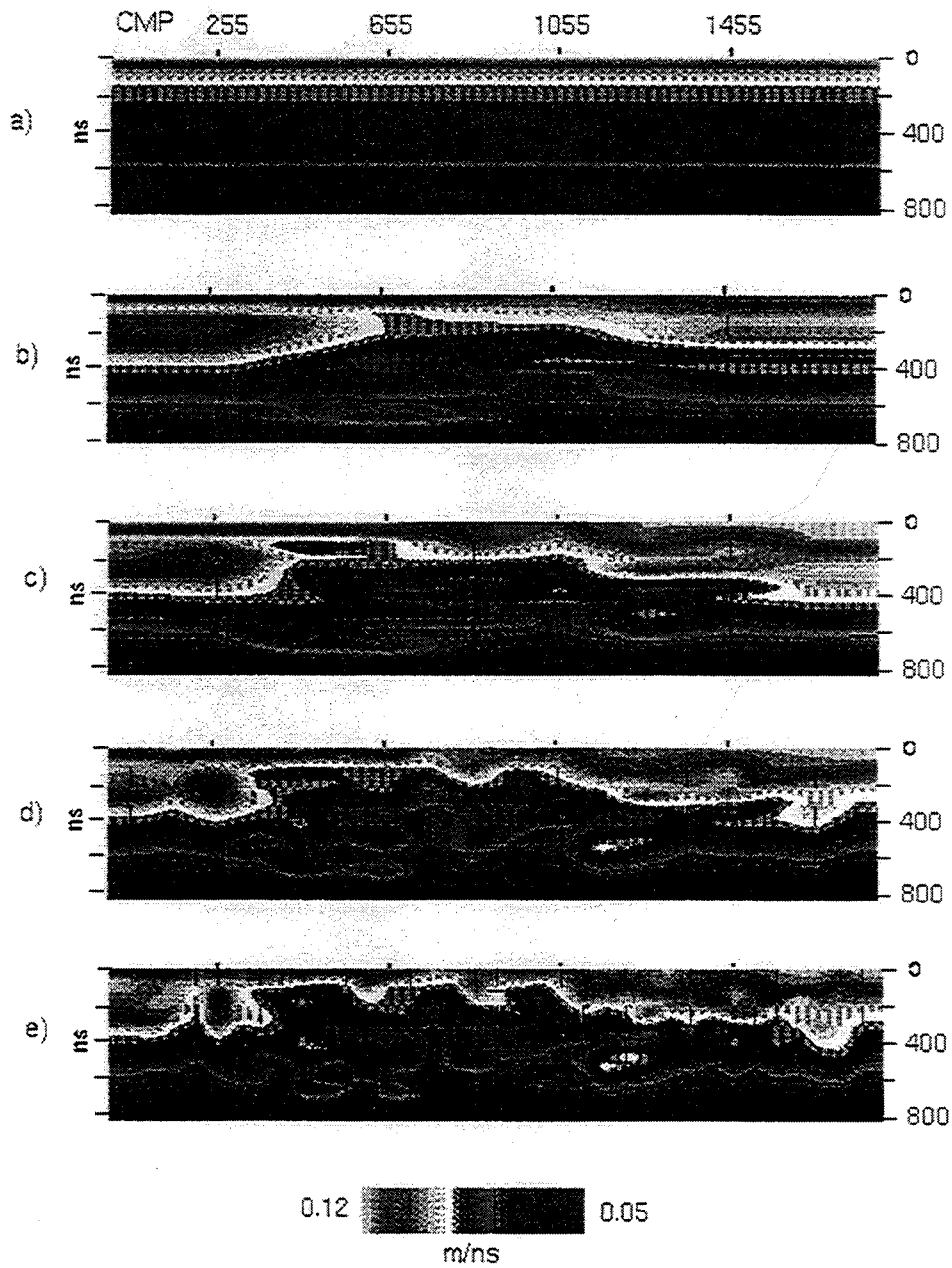
Figure 4: 2-D normal moveout velocity profile in traveltime after analysis at a) 1 CMP, b) 4 CMP's, c) 9 CMP's, d) 18 CMP's, and e) 35 CMP's.

Stacked Radar Profiles

Normal moveout corrections calculated from the NMO velocity field remove the offset dependence of the reflection traveltimes such that the data can be treated as zero offset traces. After the correction is made, the traces within each CMP are stacked to produce a single CMP trace. If the NMO correction is done with the correct velocity function, the stacked traces have an improved signal-to-noise ratio.

The NMO correction is based on the assumption that the subsurface sampled by each CMP can be adequately modeled as a sequence of horizontal layers with uniform interval velocity. Steeply dipping reflectors and strong velocity gradients test the applicability of the normal moveout and stack technique, but in general the method is sufficiently robust to improve data quality under most conditions. If lateral velocity variation is small enough, a single NMO velocity function can be used to calculate the moveout correction at all CMP's. However, where lateral velocity variation is significant, a variable NMO velocity field defined by functions at a number of CMP's must be applied to obtain the best results. In principle, an NMO velocity defined individually by velocity analysis for every CMP should yield the most accurate result. However, a spatial limit to lateral variation in NMO velocity is usually reached at some multiple CMP spacing.

NMO corrections were computed for the Chalk River data using each of the velocity fields in Figure 4. In Figure 5a we show the stacked profile when NMO is defined by a single velocity analysis (Figure 4a). Figure 5b is the stacked profile result when all thirty-five
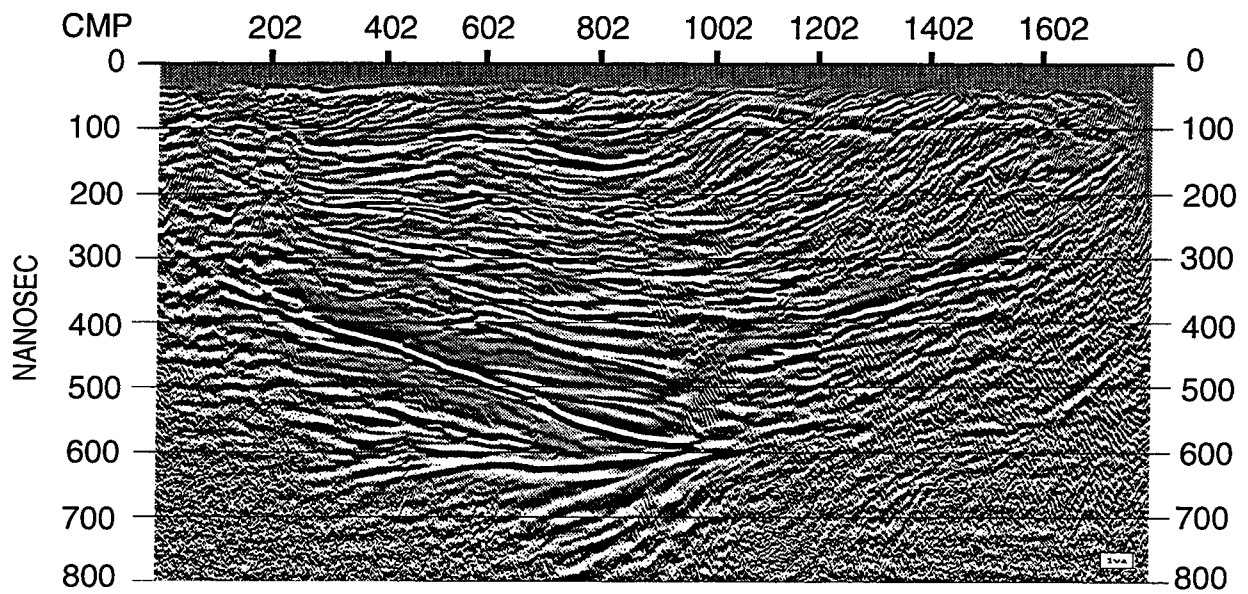
Figure 5a: CMP stacked radar reflection profile using velocity profile from 1 CMP, corresponding to Figure 4a.
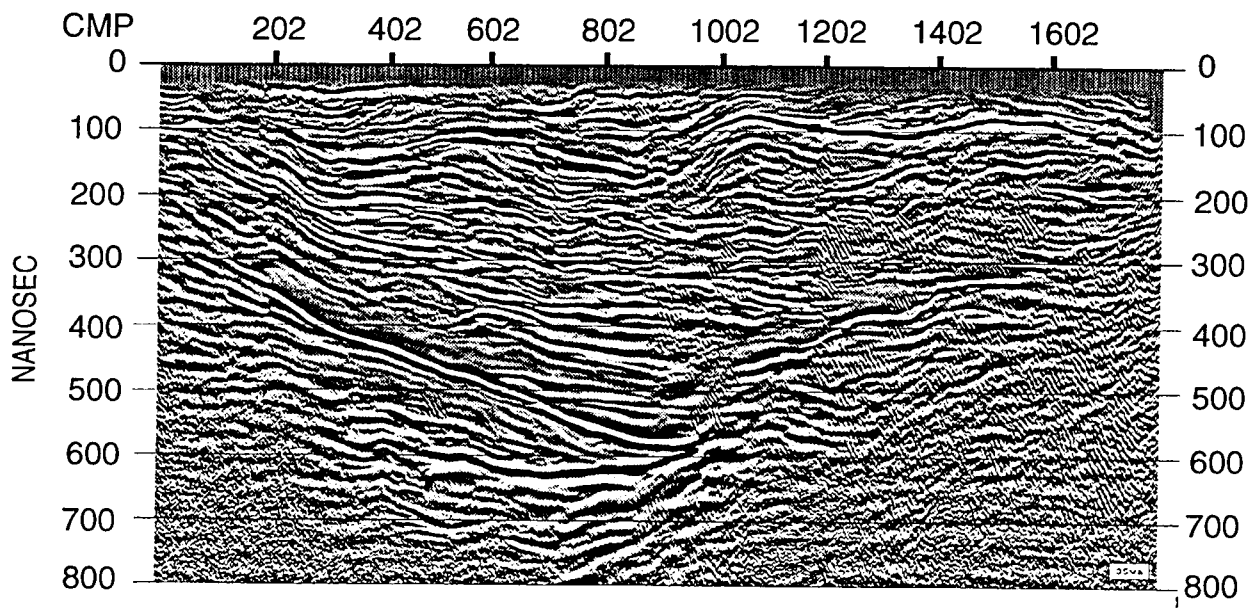
Figure 5b: CMP stacked radar reflection profile using velocity profile from 35 CMP's, corresponding to Figure 4e.

velocity analyses (Figure 4e) are used. First we compare these to the standard (no stack) profile shown in Figure 1. The stacked data profiles show a strong reduction in background noise as compared to single offset. Also, some deeper reflections, below the apparent channel bottom reflection, have been greatly enhanced, in particular, the reflector at about 600 *ns* from CMP 250 to CMP 1000. Note that when a velocity field is applied the exact traveltime to reflectors changes slightly. This is a consequence of the normal moveout correction which is shifting arrival times as a function of the particular velocity field. Comparing the single velocity stack, Figure 5a, to the multiple velocity analyses stack, Figure 5b, we observe that some deeper reflections occur down to 750 *ns* but the more clear improvement is in continuity of reflectors throughout the section. Overall, stacking with even just one velocity control point provides the major increase in the depth-of-penetration over no stack. With increasing detail in the velocity field there is some increase in the depth-of-penetration but primarily improves reflector continuity and time structure. The fact that the majority of depth-of-penetration increase occurs with the stack from even a single velocity analyses as compared to no stack, suggests that it is the multi-offset nature of the stack, in particular the far offsets, that provide the signal from the deeper reflectors.

As previously noted, the data between about 200 to 400 ns to the right of CMP 900 shows very few coherent reflectors in the standard GPR survey shown in Figure 1. In fact the left half of the profile is quite different than the right half of the profile. With the NMO correction and stack, the region on the right changes dramatically, with many reflectors

15

emerging from the stack. When only one velocity is applied, Figure 5a, this area of the data is still poorly resolved. However, when all velocity functions are included in the velocity description, the stack has improved continuity of a number of reflections from the left side of the data into the right side. Also, note that the deepest reflection on the right side, now appears to consist of a series of step-like events which may be interpreted as due to stream erosional features. Although not shown here, only small differences between the stack based on eighteen velocity analyses and thirty-six were observed. This implies that lateral velocity resolution for these data is between 50 and 100 CMP's (12.5 to 25 meters).

Radar Propagation Approximations

Radar propagation is fundamentally limited by the conductivity of the subsurface medium. Only in low-loss media can radar signals penetrate deep enough to provide a useful subsurface image. For radar, low-loss media has been described as soil or rock with conductivity less than 100 mS/m (Davis and Annan, 1989). Useful approximations for describing the propagation of radar signals can be found by considering the time harmonic solution of the equation

$$\nabla^2 \vec{E} = \mu\sigma\frac{\delta\vec{E}}{\delta t} + \mu\varepsilon\frac{\delta^2\vec{E}}{\delta t^2} \tag{1}$$

derived from Maxwell's equation for the case of a homogeneous isotropic medium. $\vec{E}$ is the electric field intensity and the constants of proportionality, ε, μ and σ are the electric permittivity, magnetic permeability and conductivity of the medium. The first term on the

right side of the wave Eq (1) represents conduction of charge due to the applied electric field. The second term describes the displacement of charge due to the field.

A solution to Eq (1) of the form

$$\vec{E}(\vec{z}, t) = \vec{E}_o e^{-\gamma z} e^{i\omega t} \tag{2}$$

yields the dispersion relation

$$k^2 = i\mu\sigma\omega + \mu\varepsilon\omega^2. \tag{3}$$

The wavenumber, k, is complex and can be written as

$$k = \alpha + i\beta \tag{4}$$

where the attenuation constant

$$\alpha = \frac{\omega}{c}\sqrt{\frac{\kappa_e}{2}\left(\sqrt{1 + \tan^2\delta} - 1\right)} \tag{5}$$

and phase constant

$$\beta = \frac{\omega}{c}\sqrt{\frac{\kappa_e}{2}\left(\sqrt{1 + \tan^2\delta} + 1\right)} \tag{6}$$

are both real. The parameters, c and κ_e are the electromagnetic velocity in free space and the real part of the dielectric constant of the medium. Relative susceptibility, $\frac{\mu}{\mu_o}$, has been eliminated since it is considered to be unity for most near surface earth materials (Telford et al., 1976). The solution to the equation can then be written as

$$\vec{E}(\vec{z}, t) = \vec{E}_o e^{-\alpha z} e^{-i(\omega t - \beta z)} \tag{7}$$

17

which is the expression for a damped plane wave propagating with phase velocity

$$v = \frac{\omega}{\beta} \qquad (8)$$

For a plane wave propagating with the angular frequency ω, the ratio of conduction current density to displacement current density is the loss tangent

$$\tan \delta = \frac{\sigma}{\omega \varepsilon}. \qquad (9)$$

In materials that are good conductors, displacement currents are negligible compared to conduction currents, and Eq (1) reduces to a diffusion equation, i.e., the fields do not propagate as electromagnetic waves. For materials with low conductivity, and when the frequency of the oscillating electric field is high enough, the displacement current dominates over the conduction current and electromagnetic waves will propagate (Stratton, 1941). For GPR systems, which by definition are high frequency, the loss tangent is very small and the diffusion term can be neglected. In this case, where $\tan \delta \ll 1$, the phase constant reduces to

$$\beta \approx \frac{\omega}{c} \sqrt{\kappa_e} \qquad (10)$$

such that

$$v \approx \frac{c}{\sqrt{\kappa_e}} \qquad (11)$$

and α reduces such that a depth of penetration, d_p, can be approximated by

$$d_p = \frac{1}{\alpha} \approx 5 \times 10^{-3} \frac{\sqrt{\kappa_e}}{\sigma} \quad meters \qquad (12)$$

Since common soil mixtures have dielectric constants less than fresh water ($\kappa_e = 80$), only very low conductivity materials ($\sigma < 100\ mS/m$) will allow propagation to useful depths. For example if $\kappa_e = 9$ then a depth of penetration of one meter requires that $\sigma = 15\ mS/m$.

This discussion has centered on the time harmonic solution to the wave equation and as such has not considered that the material properties are also frequency dependent and therefore should be treated as complex numbers. However, Davis and Annan (1989) and others have shown that in the frequency range of ground penetrating radar, 10–1000 MHz, low-loss media are essentially non-dispersive. In our interpretation we treat the dielectric constant as real and related to the propagation velocity by the simple expression found in Eq (11). In making this approximation we recognize that frequency dependence as well as many other factors such as scattering loss, source/receiver antenna power and transmission characteristics, and ground coupling (Daniels, 1989) are not being accounted for. However, our assumption is that these factors change much more slowly than dielectric constant if reflections are observed in the data.

Interval velocity and water content

To interpret the NMO velocity field derived from the multi-offset data, it is necessary to calculate interval velocities and find the relationship of radar propagation velocity to other geoelectric properties. Interval velocity $v_{i,n}$ was calculated using the Dix formula (Dix, 1955).

$$v_{i,n} = \sqrt{\frac{v_{NMO,n}^2 t_n - v_{NMO,n-1}^2 t_{n-1}}{t_n - t_{n-1}}} \qquad (13)$$

This calculation was made difficult by the fact that radar velocity decreases with increasing traveltime. The Dix formulation does not preclude the case of velocity decreasing with traveltime but we found that with decreasing velocity the numerator inside the square root of (13) can be negative if the traveltime interval is small or the NMO velocity change is large. Where this situation was encountered we used the average velocity of laterally adjacent intervals. When the Dix formula is applied to calculated exact NMO traveltimes and moveout velocities for a radar velocity model, this problem is not observed. This implies that the Dix inversion when applied to radar data is very sensitive to noise in the velocity analysis. In consideration of this, all properties calculated from the interval velocities were subjected to strong smoothing. For example, time-to-depth conversion for the profile was taken to be the least squares linear fit to the data from all of the velocity analyses.

The final step in our interpretation scheme is to relate the calculated radar interval velocities to water content. Interval velocity derived from reflection moveout curves is the group velocity, but in non-dispersive media, group velocity is equal to phase velocity and we can use the approximation (11) to convert velocity to dielectric constant. Topp *et al.* (1981) derived an empirical relationship between measured water content in laboratory samples and dielectric constant. Their empirical equation for estimating volumetric water content θ_v is

$$\theta_v = -5.3 \times 10^{-2} + 2.92 \times 10^{-2}\kappa_e - 5.5 \times 10^{-4}\kappa_e^2 + 4.3 \times 10^{-6}\kappa_e^3 \qquad (14)$$

This equation is most appropriate to GPR since it is based on measurements on soil samples of varying water content in the frequency range of ground penetrating radar systems with a laboratory setup equivalent to a pulsed radar system.

We also considered two other functions to estimate water content. The CRIM (complex refractive index method) equation is used for interpretation of electromagnetic propagation logs. It is also an empirically derived mixing law relating dielectric constant to water filled porosity, ϕ,

$$\phi_{CRIM} = \frac{\frac{\sqrt{\kappa}}{\sqrt{1-\tan^2\frac{\delta}{2}}} - \sqrt{\kappa_m}}{\frac{\sqrt{\kappa_w}}{\sqrt{1-\tan^2\frac{\delta}{2}}} - \sqrt{\kappa_m}} \tag{15}$$

where κ is the real part of the dielectric constant of the water (κ_w) and rock matrix (κ_m) mixture (Schlumberger, 1991). To apply this equation to GPR data we assume that $\tan\delta \ll 1$ for all components of the mixture so that the equation reduces to

$$\phi_{CRIM} \approx \frac{\sqrt{\kappa} - \sqrt{\kappa_m}}{\sqrt{\kappa_w} - \sqrt{\kappa_m}} \tag{16}$$

Another mixing formulation is discussed by Sen *et al.* (1981) for estimating water saturated porosity. This is the two-phase Hanai-Bruggeman equation which in the frequency range of radar can be approximated by

$$\phi_{H-B} \approx \left(\frac{\kappa_w}{\kappa}\right)^{\frac{1}{m}} \left(\frac{\kappa - \kappa_m}{\kappa_w - \kappa_m}\right) \tag{17}$$

where m in the exponent is the geometric factor from Archie's law (Samstag, 1992). This factor is most commonly taken to be $m = 2$ (Sheriff, 1991) but in Jackson *et al.* (1978) it

is empirically shown to range in marine sands from $m = 1.52$ for shaly sand to $m = 1.9$ for platey shell fragments. In saturated soils the porosity calculated from (16) or (17) is equal to the fractional water content of Eq (14). Figure 6 shows a comparison of the the water content versus dielectric constant calculated with these equations. For equations (16) and (17) we used $\kappa_w = 80$ and $\kappa_m = 4.5$ to approximate a fresh water saturated sand. The geometric factor in Eq (17) was taken to be $m = 2$ for simplicity since we are measuring quantities on a gross scale compared to the micro-geometry reflected in the m factor. From the plot we can see that any of these relationships would yield similar results in converting dielectric constant to water content but the point of this calculation is to show that the Topp Eq (14) is in good agreement with other estimation techniques. If the GPR data was collected at multiple frequencies it would be more appropriate to use the Hanai-Bruggeman equation which, in its complete form, is frequency dependent. It should also be noted that the actual measured property, interval velocity, changes more slowly with water content as velocity decreases. Since radar velocity in general decreases with depth, decreasing sensitivity of the inversion to variations in water content is expected to occur at greater depths.

We used the Topp equation to make the estimate of water content shown in Figure 7 from the interval velocity. In order to compare this plot to the reflection profiles, the water content is plotted linear in time, but with the approximate depths indicated on the right. The water content estimates were binned into 20 ns intervals and then smoothed three times with a nine point averaging window. The result shows clearly a zone of increasingly

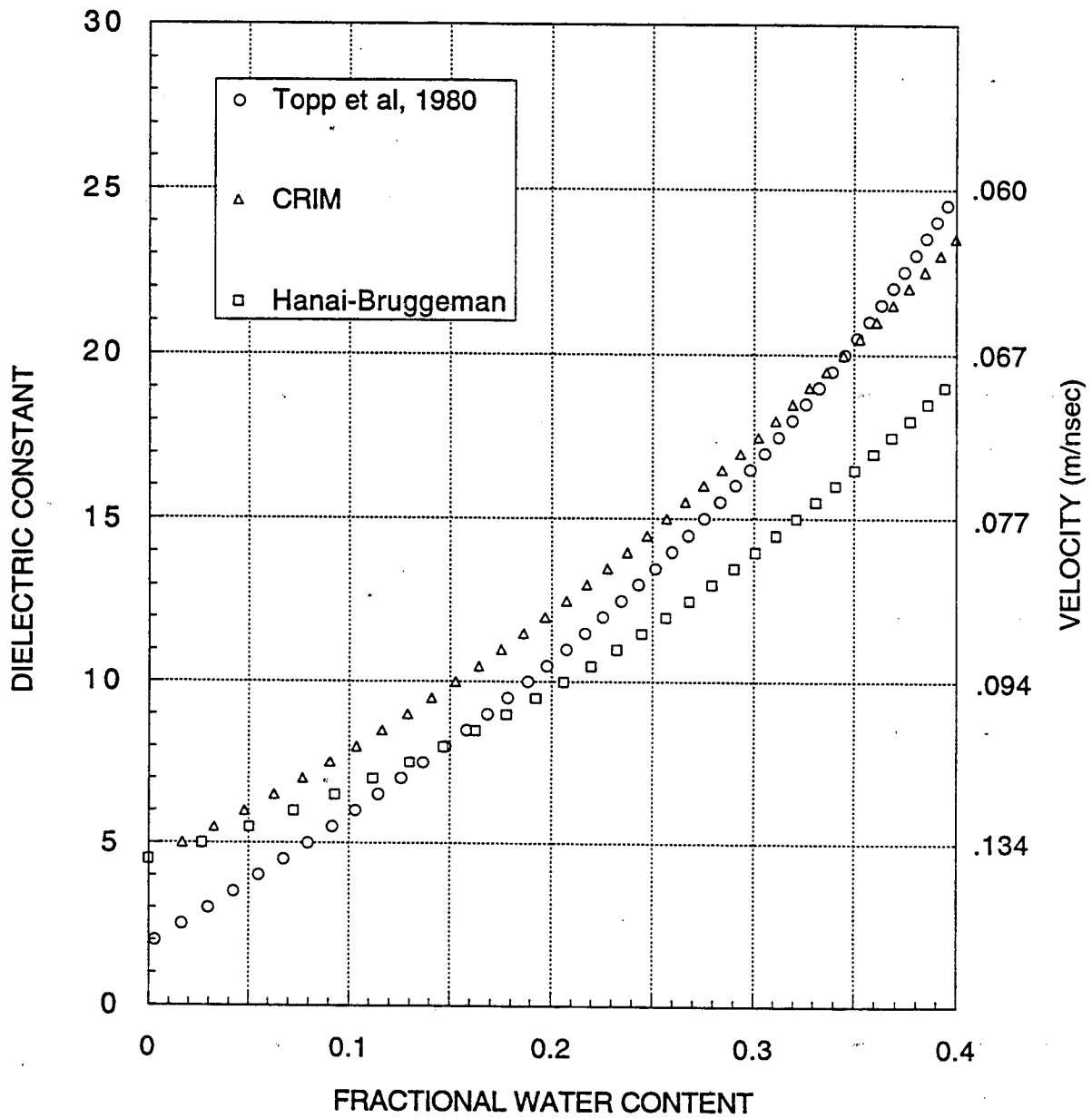Figure 6: Relating dielectric constant to water content in low-loss media. Comparison of Topp *et al.* (1981) empirical relation to the CRIM (Schlumberger, 1991) and Hanai-Bruggeman (Sen *et al.,* 1981) equations.
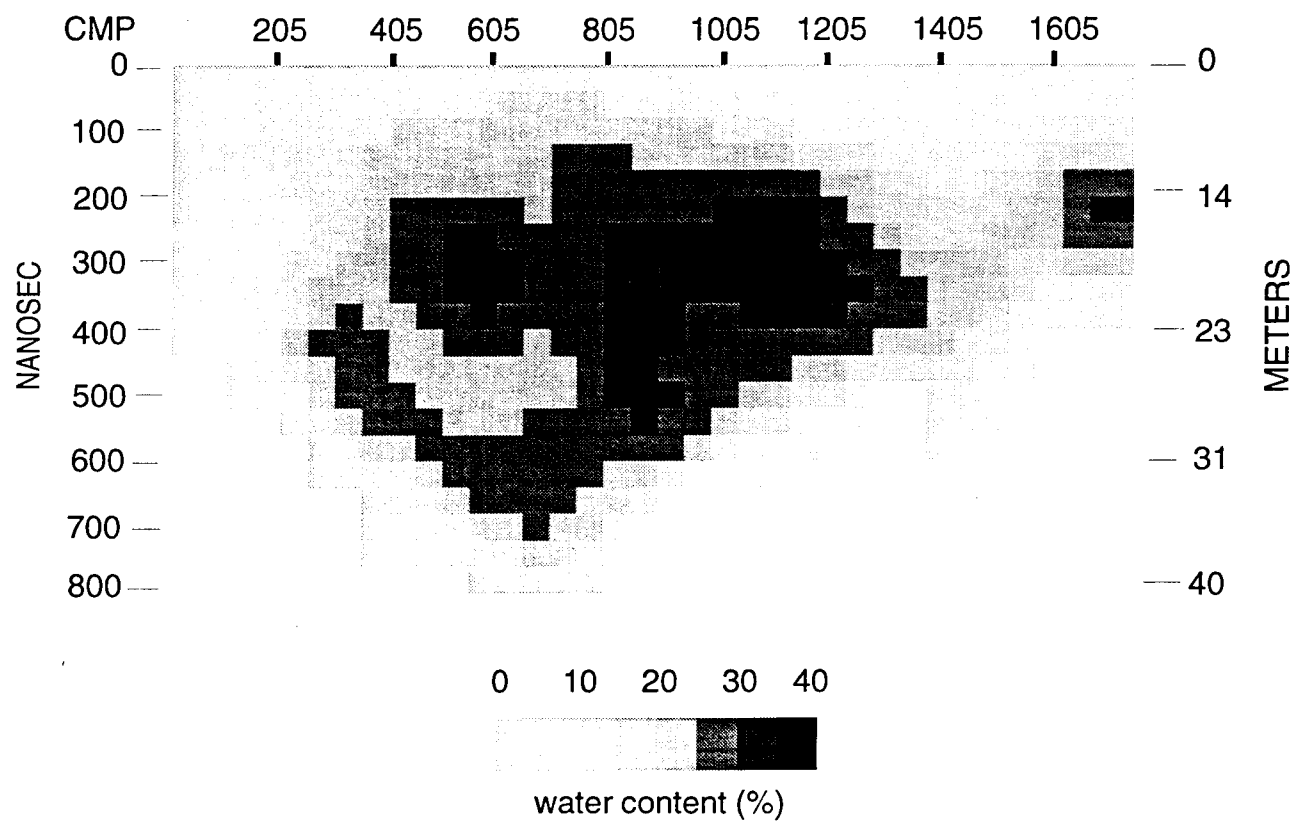
Figure 7: Water content estimated from the ground penetrating radar interval velocity using the Topp *et al.* (1981) equation. Values have been smoothed over 150 CMP's laterally and 120 nanoseconds in time.

shallow high water content from left to right along the profile. This can be interpreted as an indication of a rising water table. Since this region of high water content cuts across the detailed reflection structure, it implies that water filled porosity and permeability pathways are not constrained to apparent stratigraphic structure. Lateral variations in water content will occur within depositional units as sand and clay ratios and grain size vary. Since water distributed across stratigraphic units is not likely to be connate water, it is reasonable to conclude that the zones of high water content are also the zones of highest permeability. There is also some indication that there are areas of decreasing water content at depth which can be interpreted to be a result of differences in soil porosity determined by soil type and compaction.

Conclusion

Ground penetrating radar surveys collected with the CMP multi-offset geometry yield improved subsurface images over single offset surveys. We have shown that the CMP profile is itself improved as the number of velocity analyses is increased. This leads to the conclusion that lateral variation in radar propagation velocity can be significant even over the limited range of a typical GPR survey. The CMP stacking process yields improved depth-of-penetration over a single offset survey while detailed velocity analysis yields improvement to continuity of reflectors throughout the stacked profile.

In this study we have also attempted to connect the practical measurement of radar

velocity from the multi-offset data with the theoretical and laboratory relationships between water content and dielectric constant. We have shown a practical approach to estimating water content from these velocities based on the assumption that media conducive to radar propagation is essentially non-dispersive. The results of applying this method to the Chalk River data illustrates the method but due to the lack of comparative data, in particular field measured water content or dielectric constant, we cannot establish how accurate these results are. It should be considered for such approximations that the accuracy is no better than that of the velocity which is estimated to be within 10–20% of the average. Some improvement to this could be made by increasing the number of source to receiver offsets recorded for each CMP%. We also suggest that a test of this interpretation method should be done by measuring subsurface water content in an area while acquiring a multi-offset radar survey.

REFERENCES

Daniels, J.J., 1989, Fundamentals of ground penetrating radar, *Proc. of the Symposium on the Application of Geophysics to Engineering and Environmental Problems (SAGEEP)*, March, 1989.

Davis, J.L. and Annan, A.P., 1989, Ground penetrating radar for high resolution mapping of soil and rock stratigraphy, *Geophysical Prospecting 37*, 531–551.

Dix, C.H., 1955, Seismic velocities from surface measurements, *Geophysics 20*, 68-86.

Fisher, E., McMechan, G. and Annan, A.P., 1992, Acquisition and processing of wide-aperture ground-penetrating radar data, *Geophysics 57*, 495–504.

Gerlitz, K., Knoll, M.D., Cross, G.M., Luzitano, R.D. and Knight, R., 1993, Processing ground penetrating radar data to improve resolution of near-surface targets, *Proc. of the Symposium on the Application of Geophysics to Engineering and Environmental Problems (SAGEEP)*, 561-574.

Gudmandsen, P., 1971, Electromagnetic probing of ice, in *Electromagnetic Probing in Geophysics, J.R. Wait (ed.)*, The Golem Press, Boulder, CO., p.321-348.

Jackson, P.D., Smith, D.T., and Stanford P.N., 1978, Resistivity-porosity-particle shape relationships for marine sands, *Geophysics 43*, 1250-1268.

Samstag, F.J., 1992, An effective-medium model for complex conductivity of shaly sands in the salinity, frequency, and saturation domains, *PhD Thesis, Texas A&M University*

Schlumberger, 1991, *Log Interpretation Principles/Applications*, Schlumberger Educational

Services, Houston, Tx.

Sen, P.N., Scala, C. and Cohen, M.H., 1981, A self-similar model for sedimentary rocks with application to the dielectric constant of fused glass beads, *Geophysics 46*, 781-795.

Sheriff, R.E., 1991, *Encyclopedic Dictionary of Exploration Geophysics, 3rd Ed.*, SEG, Tulsa, OK.

Stratton, J.A., 1941, *Electromagnetic Theory*, McGraw-Hill, Inc. New York.

Telford, W.M., Geldart, L.D., Sheriff, R.E. and Keys, D.A., 1976, *Applied Geophysics*, Cambridge University Press, Cambridge.

Topp, G.C., Davis, J.L. and Annan, A.P., 1980, Electromagnetic determination of soil water content: measurements in coaxial transmission lines, *Water Resources Research 16*, 574-582.

Yilmaz, Ö., 1987, *Seismic Data Processing*, SEG, Tulsa, OK.

Prof. Thomas Ahrens
Seismological Lab, 252-21
Division of Geological & Planetary Sciences
California Institute of Technology
Pasadena, CA 91125

Prof. Keiiti Aki
Center for Earth Sciences
University of Southern California
University Park
Los Angeles, CA 90089-0741

Prof. Shelton Alexander
Geosciences Department
403 Deike Building
The Pennsylvania State University
University Park, PA 16802

Prof. Charles B. Archambeau
University of Colorado
JSPC
Campus Box 583
Boulder, CO 80309

Dr. Thomas C. Bache, Jr.
Science Applications Int'l Corp.
10260 Campus Point Drive
San Diego, CA 92121 (2 copies)

Prof. Muawia Barazangi
Cornell University
Institute for the Study of the Continent
3126 SNEE Hall
Ithaca, NY 14853

Dr. Jeff Barker
Department of Geological Sciences
State University of New York
 at Binghamton
Vestal, NY 13901

Dr. Douglas R. Baumgardt
ENSCO, Inc
5400 Port Royal Road
Springfield, VA 22151-2388

Dr. Susan Beck
Department of Geosciences
Building #77
University of Arizona
Tuscon, AZ 85721

Dr. T.J. Bennett
S-CUBED
A Division of Maxwell Laboratories
11800 Sunrise Valley Drive, Suite 1212
Reston, VA 22091

Dr. Robert Blandford
 AFTAC/TT, Center for Seismic Studies
1300 North 17th Street
Suite 1450
Arlington, VA 22209-2308

Dr. Stephen Bratt
ARPA/NMRO
3701 North Fairfax Drive
Arlington, VA 22203-1714

Dale Breding
U.S. Department of Energy
Recipient, IS-20, GA-033
Office of Arms Control
Washington, DC 20585

Dr. Lawrence Burdick
C/O Barbara Wold
Dept of Biology
CA Inst. of Technology
Pasadena, CA 91125

Dr. Robert Burridge
Schlumberger-Doll Research Center
Old Quarry Road
Ridgefield, CT 06877

Dr. Jerry Carter
Center for Seismic Studies
1300 North 17th Street
Suite 1450
Arlington, VA 22209-2308

Dr. Martin Chapman
Department of Geological Sciences
Virginia Polytechnical Institute
21044 Derring Hall
Blacksburg, VA 24061

Mr Robert Cockerham
Arms Control & Disarmament Agency
320 21st Street North West
Room 5741
Washington, DC 20451,

Prof. Vernon F. Cormier
Department of Geology & Geophysics
U-45, Room 207
University of Connecticut
Storrs, CT 06268

Prof. Steven Day
Department of Geological Sciences
San Diego State University
San Diego, CA 92182

Dr. Zoltan Der
ENSCO, Inc.
5400 Port Royal Road
Springfield, VA 22151-2388

Dr. Stanley K. Dickinson
AFOSR/NM
110 Duncan Avenue
Suite B115
Bolling AFB, DC 20332-6448

Prof. Adam Dziewonski
Hoffman Laboratory, Harvard University
Dept. of Earth Atmos. & Planetary Sciences
20 Oxford Street
Cambridge, MA 02138

Prof. John Ebel
Department of Geology & Geophysics
Boston College
Chestnut Hill, MA 02167

Dr. Petr Firbas
Institute of Physics of the Earth
Masaryk University Brno
Jecna 29a
612 46 Brno, Czech Republic

Dr. Mark D. Fisk
Mission Research Corporation
735 State Street
P.O. Drawer 719
Santa Barbara, CA 93102

Prof. Donald Forsyth
Department of Geological Sciences
Brown University
Providence, RI 02912

Dr. Cliff Frolich
Institute of Geophysics
8701 North Mopac
Austin, TX 78759

Dr. Holly Given
IGPP, A-025
Scripps Institute of Oceanography
University of California, San Diego
La Jolla, CA 92093

Dr. Jeffrey W. Given
SAIC
10260 Campus Point Drive
San Diego, CA 92121

Dr. Dale Glover
Defense Intelligence Agency
ATTN: ODT-1B
Washington, DC 20301

Dr. Indra N. Gupta
Multimax, Inc.
1441 McCormick Drive
Landover, MD 20785

Dan N. Hagedon
Pacific Northwest Laboratories
Battelle Boulevard
Richland, WA 99352

Dr. James Hannon
Lawrence Livermore National Laboratory
P.O. Box 808, L-205
Livermore, CA 94550

Dr. Roger Hansen
University of Colorado, JSPC
Campus Box 583
Boulder, CO 80309

Prof. David G. Harkrider
Division of Geological & Planetary Sciences
California Institute of Technology
Pasadena, CA 91125

Prof. Danny Harvey
University of Colorado, JSPC
Campus Box 583
Boulder, CO 80309

Prof. Donald V. Helmberger
Division of Geological & Planetary Sciences
California Institute of Technology
Pasadena, CA 91125

Prof. Eugene Herrin
Geophysical Laboratory
Southern Methodist University
Dallas, TX 75275

Prof. Robert B. Herrmann
Department of Earth & Atmospheric Sciences
St. Louis University
St. Louis, MO 63156

Prof. Lane R. Johnson
Seismographic Station
University of California
Berkeley, CA 94720

Prof. Thomas H. Jordan
Department of Earth, Atmospheric &
 Planetary Sciences
Massachusetts Institute of Technology
Cambridge, MA 02139

Prof. Alan Kafka
Department of Geology & Geophysics
Boston College
Chestnut Hill, MA 02167

Robert C. Kemerait
ENSCO, Inc.
445 Pineda Court
Melbourne, FL 32940

U.S. Dept of Energy
Max Koontz, NN-20, GA-033
Office of Research and Develop.
1000 Independence Avenue
Washington, DC 20585

Dr. Richard LaCoss
MIT Lincoln Laboratory, M-200B
P.O. Box 73
Lexington, MA 02173-0073

Dr. Fred K. Lamb
University of Illinois at Urbana-Champaign
Department of Physics
1110 West Green Street
Urbana, IL 61801

Prof. Charles A. Langston
Geosciences Department
403 Deike Building
The Pennsylvania State University
University Park, PA 16802

Jim Lawson, Chief Geophysicist
Oklahoma Geological Survey
Oklahoma Geophysical Observatory
P.O. Box 8
Leonard, OK 74043-0008

Prof. Thorne Lay
Institute of Tectonics
Earth Science Board
University of California, Santa Cruz
Santa Cruz, CA 95064

Dr. William Leith
U.S. Geological Survey
Mail Stop 928
Reston, VA 22092

Mr. James F. Lewkowicz
Phillips Laboratory/GPE
29 Randolph Road
Hanscom AFB, MA 01731-3010(2 copies)

Prof. L. Timothy Long
School of Geophysical Sciences
Georgia Institute of Technology
Atlanta, GA 30332

Dr. Randolph Martin, III
New England Research, Inc.
76 Olcott Drive
White River Junction, VT 05001

Dr. Robert Masse
Denver Federal Building
Box 25046, Mail Stop 967
Denver, CO 80225

Dr. Gary McCartor
Department of Physics
Southern Methodist University
Dallas, TX 75275

Prof. Thomas V. McEvilly
Seismographic Station
University of California
Berkeley, CA 94720

Dr. Art McGarr
U.S. Geological Survey
Mail Stop 977
U.S. Geological Survey
Menlo Park, CA 94025

Dr. Keith L. McLaughlin
S-CUBED
A Division of Maxwell Laboratory
P.O. Box 1620
La Jolla, CA 92038-1620

Stephen Miller & Dr. Alexander Florence
SRI International
333 Ravenswood Avenue
Box AF 116
Menlo Park, CA 94025-3493

3

Prof. Bernard Minster
IGPP, A-025
Scripps Institute of Oceanography
University of California, San Diego
La Jolla, CA 92093

Prof. Brian J. Mitchell
Department of Earth & Atmospheric Sciences
St. Louis University
St. Louis, MO 63156

Mr. Richard J. Morrow
USACDA/IVI
320 21st St. N.W.
Washington , DC 20451

Mr. Jack Murphy
S-CUBED
A Division of Maxwell Laboratory
11800 Sunrise Valley Drive, Suite 1212
Reston, VA 22091 (2 Copies)

Dr. Keith K. Nakanishi
Lawrence Livermore National Laboratory
L-025
P.O. Box 808
Livermore, CA 94550

Prof. John A. Orcutt
IGPP, A-025
Scripps Institute of Oceanography
University of California, San Diego
La Jolla, CA 92093

Prof. Jeffrey Park
Kline Geology Laboratory
P.O. Box 6666
New Haven, CT 06511-8130

Dr. Howard Patton
Lawrence Livermore National Laboratory
L-025
P.O. Box 808
Livermore, CA 94550

Dr. Frank Pilotte
HQ AFTAC/TT
1030 South Highway A1A
Patrick AFB, FL 32925-3002

Dr. Jay J. Pulli
Radix Systems, Inc.
201 Perry Parkway
Gaithersburg, MD 20877

Dr. Robert Reinke
ATTN: FCTVTD
Field Command
Defense Nuclear Agency
Kirtland AFB, NM 87115

Prof. Paul G. Richards
Lamont-Doherty Earth Observatory
   of Columbia University
Palisades, NY 10964

Mr. Wilmer Rivers
Teledyne Geotech
1300 17th St N #1450
Arlington, VA 22209-3803

Dr. Alan S. Ryall, Jr.
ARPA/NMRO
3701 North Fairfax Drive
Arlington, VA 22203-1714

Dr.Chandan K. Saikia
Woodward Clyde- Consultants
566 El Dorado Street
Pasadena, CA 91101

Dr. Richard Sailor
TASC, Inc.
55 Walkers Brook Drive
Reading, MA 01867

Prof. Charles G. Sammis
Center for Earth Sciences
University of Southern California
University Park
Los Angeles, CA 90089-0741

Prof. Christopher H. Scholz
Lamont-Doherty Earth Observatory
   of Columbia University
Palisades, NY 10964

Dr. Susan Schwartz
Institute of Tectonics
1156 High Street
Santa Cruz, CA 95064

Mr. Dogan Seber
Cornell University
Inst. for the Study of the Continent
3130 SNEE Hall
Ithaca, NY 14853-1504

4

Secretary of the Air Force
(SAFRD)
Washington, DC 20330

Office of the Secretary of Defense
DDR&E
Washington, DC 20330

Thomas J. Sereno, Jr.
Science Application Int'l Corp.
10260 Campus Point Drive
San Diego, CA 92121

Dr. Michael Shore
Defense Nuclear Agency/SPSS
6801 Telegraph Road
Alexandria, VA 22310

Dr. Robert Shumway
University of California Davis
Division of Statistics
Davis, CA 95616

Dr. Matthew Sibol
Virginia Tech
Seismological Observatory
4044 Derring Hall
Blacksburg, VA 24061-0420

Prof. David G. Simpson
IRIS, Inc.
1616 North Fort Myer Drive
Suite 1050
Arlington, VA 22209

Donald L. Springer
Lawrence Livermore National Laboratory
L-025
P.O. Box 808
Livermore, CA 94550

Dr. Jeffrey Stevens
S-CUBED
A Division of Maxwell Laboratory
P.O. Box 1620
La Jolla, CA 92038-1620

Prof. Brian Stump
Los Alamos National Laboratory
EES-3
 Mail Stop C-335
Los Alamos, NM 87545

Prof. Jeremiah Sullivan
University of Illinois at Urbana-Champaign
Department of Physics
1110 West Green Street
Urbana, IL 61801

Prof. L. Sykes
Lamont-Doherty Earth Observatory
 of Columbia University
Palisades, NY 10964

Dr. David Taylor
ENSCO, Inc.
445 Pineda Court
Melbourne, FL 32940

Dr. Steven R. Taylor
Los Alamos National Laboratory
P.O. Box 1663
Mail Stop C335
Los Alamos, NM 87545

Prof. Tuncay Taymaz
Istanbul Technical University
Dept. of Geophysical Engineering
Mining Faculty
Maslak-80626, Istanbul Turkey

Prof. Clifford Thurber
University of Wisconsin-Madison
Department of Geology & Geophysics
1215 West Dayton Street
Madison, WS 53706

Prof. M. Nafi Toksoz
Earth Resources Lab
Massachusetts Institute of Technology
42 Carleton Street
Cambridge, MA 02142

Dr. Larry Turnbull
CIA-OSWR/NED
Washington, DC 20505

Dr. Gregory van der Vink
IRIS, Inc.
1616 North Fort Myer Drive
Suite 1050
Arlington, VA 22209

Dr. Karl Veith
EG&G
5211 Auth Road
Suite 240
Suitland, MD 20746

5

Prof. Terry C. Wallace
Department of Geosciences
Building #77
University of Arizona
Tuscon, AZ 85721

Dr. Thomas Weaver
Los Alamos National Laboratory
P.O. Box 1663
Mail Stop C335
Los Alamos, NM 87545

Dr. William Wortman
Mission Research Corporation
8560 Cinderbed Road
Suite 700
Newington, VA 22122

Prof. Francis T. Wu
Department of Geological Sciences
State University of New York
 at Binghamton
Vestal, NY 13901

Prof Ru-Shan Wu
University of California, Santa Cruz
Earth Sciences Department
Santa Cruz, CA 95064

ARPA, OASB/Library
3701 North Fairfax Drive
Arlington, VA 22203-1714

HQ DNA
ATTN: Technical Library
Washington, DC 20305

Defense Technical Information Center
Cameron Station
Alexandria, VA 22314 (2 Copies)

TACTEC
Battelle Memorial Institute
505 King Avenue
Columbus, OH 43201 (Final Report)

Phillips Laboratory
ATTN: XPG
29 Randolph Road
Hanscom AFB, MA 01731-3010

Phillips Laboratory
ATTN: GPE
29 Randolph Road
Hanscom AFB, MA 01731-3010

Phillips Laboratory
ATTN: TSML
5 Wright Street
Hanscom AFB, MA 01731-3004

Phillips Laboratory
ATTN: PL/SUL
3550 Aberdeen Ave SE
Kirtland, NM 87117-5776 (2 copies)

Dr. Michel Bouchon
I.R.I.G.M.-B.P. 68
38402 St. Martin D'Heres
Cedex, FRANCE

Dr. Michel Campillo
Observatoire de Grenoble
I.R.I.G.M.-B.P. 53
38041 Grenoble, FRANCE

Dr. Kin Yip Chun
Geophysics Division
Physics Department
University of Toronto
Ontario, CANADA

Prof. Hans-Peter Harjes
Institute for Geophysic
Ruhr University/Bochum
P.O. Box 102148
4630 Bochum 1, GERMANY

Prof. Eystein Husebye
NTNF/NORSAR
P.O. Box 51
N-2007 Kjeller, NORWAY

David Jepsen
Acting Head, Nuclear Monitoring Section
Bureau of Mineral Resources
Geology and Geophysics
G.P.O. Box 378, Canberra, AUSTRALIA

Ms. Eva Johannisson
Senior Research Officer
FOA
S-172 90 Sundbyberg, SWEDEN

Dr. Peter Marshall
Procurement Executive
Ministry of Defense
Blacknest, Brimpton
Reading FG7-FRS, UNITED KINGDOM

Dr. Bernard Massinon, Dr. Pierre Mechler
Societe Radiomana
27 rue Claude Bernard
75005 Paris, FRANCE (2 Copies)

Dr. Svein Mykkeltveit
NTNT/NORSAR
P.O. Box 51
N-2007 Kjeller, NORWAY (3 Copies)

Prof. Keith Priestley
University of Cambridge
Bullard Labs, Dept. of Earth Sciences
Madingley Rise, Madingley Road
Cambridge CB3 OEZ, ENGLAND

Dr. Jorg Schlittenhardt
Federal Institute for Geosciences & Nat'l Res.
Postfach 510153
D-30631 Hannover , GERMANY

Dr. Johannes Schweitzer
Institute of Geophysics
Ruhr University/Bochum
P.O. Box 1102148
4360 Bochum 1, GERMANY

Trust & Verify
VERTIC
Carrara House
20 Embankment Place
London WC2N 6NN, ENGLAND